Randomized Dynamic Mode Decomposition for Oscillation Modal Analysis

Abdullah Alassaf , *Student Member, IEEE,* Lingling Fan , *Senior Member, IEEE*

***Abstract*—The objective of this research is to identify oscillation modes from real-world measurement data captured by phasor measurement units (PMUs) and make distinction of their characteristics. To this end, dynamic mode decomposition (DMD) is applied. This paper improves DMD performance by data stacking. This enables DMD to accurately identify system eigenvalues and reconstruct signals in the time-evolving format. While data stacking raises the computation cost, we further implement a randomization technique for DMD to radically reduce the size of the data matrix. The randomized DMD (rDMD) is shown to achieve both efficiency in computing and accuracy in mode identification. PMU data from three real-world oscillation events are used for demonstration.**

***Index Terms*—Power system oscillations, system identification, dynamic mode decomposition, randomized technique, real-world event.**

I. Introduction

POWER system inter-area oscillation is an electromechanical behavior that exists in any interconnection system that contains more than a synchronous generator. Even with the regular operation, oscillations are found in the electric grid due to mundane actions such as load change. Oscillations with poor or negative damping could result in blackout. One such example is the August 1996 west system inter-area oscillations [1]. With PMUs installed, many oscillation events have been recorded by PMUs [2]. The communication structure of wide-area monitoring system (WAMS) can be centralized and decentralized. The latter strategy has higher efficiency and reliability [3]. An IEEE PES task force on oscillation source location was formed in 2016 with test cases from real-world events collected and available at public domain [4], [5].

To identify oscillation modes, several data-driven methods have been utilized for power system events: Prony [6], [7], [8], Matrix Pencil [9], [7], Eigensystem Realization Algorithm (ERA) [10], Koopman Analysis [11], and Variable Projection Method [12].

In the 2012 IEEE PES taskforce report on electromechanical mode identification [13], three methods for ringdown signals: Prony, Matrix Pencil, and ERA methods, were presented. Reference [14] further compares the three methods on their similarity, including data matrix formulation and noise handling relying on singular value decomposition (SVD). Case studies on two real-world events taken from [4] show ERA has the best performance in eigenvalue identification accuracy.

A more recent method called dynamic mode decomposition (DMD) has been proposed and applied in fluid community [15] in 2010. The DMD algorithm has been used in diverse applications such as brain modelling, fluid experiments, foreground/background video separation, flows around a high-speed train, and financial trading strategies [16].

DMD is applied in power systems for oscillation analysis in [17]. The authors show that DMD is more efficient than both Koopman and Prony in identifying dynamical modes and their spatial and temporal characteristics. Reference [18] visualizes the identified modes to approach more intuitive dynamical attributes. In decentralized WAMS structure, [19] successfully circumvents high-dimensional data processing using DMD Compressed Sensing that selects the most observable PMUs.

In the authors' prior work [20], DMD is applied to identify the dynamics matrix for an RLC circuit using measurement data and identify a signal's frequency components and magnitudes. The latter application achieves the same function as fast Fourier transformation (FFT). DMD and ERA have been compared in [20] to show that they achieve similar level of accuracy. The DMD extracts distortion harmonic components of microgrids [21]. Reference [22] enhances the performance of the extended DMD under noisy measurements.

For practical interest, besides eigenvalue identification, distinction of the oscillation mode as local or inter-area is desired. If the definition of the state variables is known, mode shape or eigenvector can lead to more information regarding who is contributing to the oscillation.

Compared to several other methods that rely on Hankel matrices, e.g., Prony analysis, Matrix Pencil, and ERA, DMD has a unique advantage: state variables have clear physical definition. Thus the mode shape information from the system matrix A leads to physical interpretation of how measurement influences an oscillation mode. Matrix Pencil and Prony analysis do not lead to system matrix A. Though ERA leads to a state matrix, the state variables are unknown.

DMD decomposes high-dimensional data into spatial and temporal structures. Essentially, DMD carries out eigen-decomposition for a data matrix. Hence, a data matrix can be factorized into two components: spatial and temporal. The dynamic system model can be found by keeping the dominant spatiotemporal structures which are identified using dominant singular values. This feature also helps to obtain reduced-order model which keeps only dominant eigenvalues. The future state may be predicted using the identified eigenvalues and initial states.

A. Alassaf is is with the Department of Electrical Engineering, University of Hail, Hail 55476, Saudi Arabia, and also with the Department of Electrical Engineering, University of South Florida, Tampa, FL 33620, USA (e-mail: alassaf@usf.edu).

L. Fan is with the Department of Electrical Engineering, University of South Florida, Tampa, FL 33620, USA (e-mail: linglingfan@usf.edu).

The scope of this paper is to use DMD from real-world PMU data to identify oscillation modes and distinct their nature using mode shape.

The contribution of this paper is three-fold.

- Compared to the major reference on DMD application in power system oscillation analysis [17], this paper improves DMD implementation in signal reconstruction and DMD's performance in accuracy. (i) We not only implemented DMD to identify eigenvalues from PMU measurements, but also reconstructed signals and can predict signals at any time t. This is realized by carrying out one more step to represent a data matrix's time evolving characteristics. (ii) DMD's performance is improved by data stacking technique. Accuracy in eigenvalue identification and measurement signal reconstruction has been greatly improved. Comparison of without and with data stacking technique is presented in this paper.
- With data stacking technique, the row dimension of the data matrix increases significantly. This causes more computing cost. We implement randomization technique into DMD [23] and radically reduce the matrix dimension. In turn, computing efficiency of DMD-based oscillation modal identification has been greatly improved.
- Relying on synchrophasor measurements collected by a region from scattered locations, distinction between system wide oscillation mode and regional oscillation mode can be made based on identified mode shapes associated with the measurements at different locations. PMU measurements from real-world oscillation events were used for this research. The analysis results match the knowledge of those real-world oscillations. The proposed method has been compared with the existing methods that are Prony, Matrix Pencil, and ERA in case studies.

The rest of this paper is organized as follows. Section II reviews DMD and points out the difference of data matrix reconstruction in this paper and [17]. Section III presents Randomized Dynamic Mode Decomposition (rDMD). The DMD and rDMD are implemented on real-world event data analysis in Section IV. Section V concludes the paper.

II. Dynamic Mode Decomposition

In linear or linearized dynamic system, the dynamics matrix, $\mathbf{A} \in \mathbb{R}^{n\times n}$, maps the snapshot $\mathbf{x}_k$ to the subsequent snapshot $\mathbf{x}_{k+1}$ as

$$\mathbf{x}_{k+1} = \mathbf{A}\mathbf{x}_k. \tag{1}$$

where $\mathbf{x} \in \mathbb{R}^n$. The time interval between two consecutive snapshots is Δt.

Applying eigen-decomposition to matrix $\mathbf{A} = \mathbf{\Phi\Lambda\Phi}^{-1}$ leads to

$$\mathbf{x}_{k+1} = \mathbf{\Phi\Lambda\Phi}^{-1}\mathbf{x}_k = \mathbf{\Phi\Lambda^2\Phi}^{-1}\mathbf{x}_{k-1} = \cdots = \mathbf{\Phi\Lambda}^k \underbrace{\mathbf{\Phi}^{-1}\mathbf{x}_1}_{\mathbf{b}}. \tag{2}$$

where $\mathbf{b} \in \mathbb{C}^{n\times 1}$, $\mathbf{\Phi} \in \mathbb{C}^{n\times n}$ is the right eigenvector matrix of $\mathbf{A}$, and $\mathbf{\Lambda}$ is a diagonal matrix with elements as $\lambda_i, i = 1, \cdots, n$.

Equation (2) can also be written as follows.

$$\mathbf{x}_{k+1} = \sum_{j=1}^{n} \boldsymbol{\phi}_j \lambda_j^k b_j, \tag{3}$$

The time-domain expression of $\mathbf{x}(t)$ can also be constructed using the eigenvalues and eigenvectors of $\mathbf{A}$.

$$\mathbf{x}(t) = \sum_{j=1}^{n} \boldsymbol{\phi}_j e^{\omega_j t} b_j = \mathbf{\Phi} e^{\mathbf{\Omega} t}\mathbf{b}. \tag{4}$$

where $\mathbf{\Omega}$ is a diagonal matrix that contains the continuous-eigenvalues, ω_j. The relationship between the discrete and continuous eigenvalue is $\omega_j = \ln(\lambda_j)/\Delta t$.

The eigenvector matrix $\mathbf{\Phi}$, the eigenvalue matrix $\mathbf{\Lambda}$, and the initial state projected to the eigenvector basis $\mathbf{b}$ will all be identified from the measurement data by DMD.

In DMD, a data matrix $\mathbf{X}$ is constructed to contain state for m snapshots with equal time-intervals.

$$\mathbf{X} = \begin{bmatrix} | & | & & | \\ \mathbf{x}_1 & \mathbf{x}_2 & \cdots & \mathbf{x}_m \\ | & | & & | \end{bmatrix}. \tag{5}$$

$\mathbf{X}$ can be expressed using (2):

$$\mathbf{X} = \mathbf{\Phi}\begin{bmatrix} \mathbf{b} & \mathbf{\Lambda b} & \cdots & \mathbf{\Lambda}^m\mathbf{b} \end{bmatrix}. \tag{6}$$

In (6), multiplication of a diagonal matrix $\mathbf{\Lambda}$ with a column vector $\mathbf{b}$ is equivalent to $\mathrm{diag}(\mathbf{b})\,\mathrm{col}(\mathbf{\Lambda})$. Hence, (6) can be expressed:

$$\mathbf{X} = \begin{bmatrix} | & | & \\ \boldsymbol{\phi}_1 & \boldsymbol{\phi}_2 & \cdots \\ | & | & \end{bmatrix} \mathrm{diag}(\mathbf{b}) \begin{bmatrix} 1 & \lambda_1 & \cdots & \lambda_1^m \\ 1 & \lambda_2 & \cdots & \lambda_2^m \\ \vdots & \vdots & \ddots & \vdots \end{bmatrix}. \tag{7}$$

It has to be noted that while eigenvalues and $\mathbf{\Phi}$ were identified in [17], identification $\mathbf{b}$ was not carried out. In [17], the data matrix $\mathbf{X}$ is decomposed as $\mathbf{X} = \mathbf{\Phi\Lambda\Gamma}$ (Equation (28) of [17]). Though $\mathbf{\Lambda}$ has been identified, the time-evolving characteristics have not been explicitly identified. Thus, prediction of state at a future time is not possible.

In the following, the procedure of identifying $\mathbf{\Phi}$, $\mathbf{\Lambda}$, and $\mathbf{b}$ from $\mathbf{X}$ is given.

First, the collected snapshots of measurements are gathered in two sequential overlapping sets that one of them is time-shifted, as follows.

$$\mathbf{X}_1^{m-1} = \begin{bmatrix} | & | & & | \\ \mathbf{x}_1 & \mathbf{x}_2 & \cdots & \mathbf{x}_{m-1} \\ | & | & & | \end{bmatrix}, \tag{8a}$$

$$\mathbf{X}_2^{m} = \begin{bmatrix} | & | & & | \\ \mathbf{x}_2 & \mathbf{x}_3 & \cdots & \mathbf{x}_{m} \\ | & | & & | \end{bmatrix}, \tag{8b}$$

where $\mathbf{X}_1^{m-1} \in \mathbb{R}^{n\times(m-1)}$, $\mathbf{X}_2^{m} \in \mathbb{R}^{n\times(m-1)}$. The subscript and superscript refer to the first and last measurement snapshots in set, respectively. It can be seen that

$$\mathbf{X}_2^m = \mathbf{A}\mathbf{X}_1^{m-1}.$$

$\mathbf{A}$ can be found as

$$\mathbf{A} = \mathbf{X}_2^m (\mathbf{X}_1^{m-1})^\dagger, \tag{9}$$

where superscript † notates Moore-Penrose pseudo inverse that is mathematically evaluated as $\mathbf{X}^\dagger = (\mathbf{X}^T\mathbf{X})^{-1}\mathbf{X}^T$, where the superscript T refers to the transpose. To avoid dealing with inverse of a large-size matrix, Singular Value Decomposition (SVD) is adopted for $\mathbf{X}_1^{m-1}$. In addition, a rank r will be chosen for rank reduction. Hence,

$$\mathbf{X}_1^{m-1} \approx \mathbf{U}\mathbf{\Sigma}\mathbf{V}^*, \tag{10}$$

where $\mathbf{U} \in \mathbb{R}^{n\times r}, \mathbf{\Sigma} \in \mathbb{R}^{r\times r}$, and $\mathbf{V} \in \mathbb{R}^{(m-1)\times r}$, and $*$ denotes the complex conjugate transpose. $\mathbf{U}$ and $\mathbf{V}$ are unitary matrices, they satisfy $\mathbf{U}^*\mathbf{U} = \mathbf{I}$ and $\mathbf{V}^*\mathbf{V} = \mathbf{I}$.

It can be found from (10) that the pseudo-inverse of $\mathbf{X}_1^{m-1}$ can be expressed as:

$$(\mathbf{X}_1^{m-1})^\dagger \approx \mathbf{V}\mathbf{\Sigma}^{-1}\mathbf{U}^*. \tag{11}$$

Hence, according to (9), $\mathbf{A}$ can be expressed as follows.

$$\mathbf{A} = \mathbf{X}_2^m \mathbf{V}\mathbf{\Sigma}^{-1}\mathbf{U}^*, \tag{12}$$

A low-dimensional dynamics matrix $\tilde{\mathbf{A}}$ is realized by projecting $\mathbf{A}$ onto $\mathbf{U}$ basis:

$$\tilde{\mathbf{A}} = \mathbf{U}^*\mathbf{A}\mathbf{U} = \mathbf{U}^*\mathbf{X}_2^m\mathbf{V}\mathbf{\Sigma}^{-1}, \tag{13}$$

where $\tilde{\mathbf{A}} \in \mathbb{R}^{r\times r}$. The low-rank dynamical model becomes:

$$\tilde{\mathbf{x}}_{k+1} = \tilde{\mathbf{A}}\tilde{\mathbf{x}}_k. \tag{14}$$

where $\tilde{\mathbf{x}} = \mathbf{U}^*\mathbf{x}$ and $\tilde{\mathbf{x}} \in \mathbb{R}^r$.

The full-rank state vector can be recovered by $\mathbf{x}_k = \mathbf{U}\tilde{\mathbf{x}}_k$.

Next, the eigendecomposition of the low-dimensional dynamics matrix $\tilde{\mathbf{A}}$ is carried out.

$$\tilde{\mathbf{A}}\mathbf{W} = \mathbf{W}\mathbf{\Lambda}, \tag{15}$$

where $\mathbf{\Lambda} \in \mathbb{C}^{r\times r}$, and $\mathbf{W} \in \mathbb{C}^{r\times r}$. The diagonal entries of $\mathbf{\Lambda}$ are the eigenvalues, and the columns of $\mathbf{W}$ are the eigenvectors. While $\mathbf{\Lambda}$ is associated to both $\tilde{\mathbf{A}}$ and $\mathbf{A}$, $\mathbf{W}$ is associated to only $\tilde{\mathbf{A}}$. The eigenvectors of the high-dimensional dynamics matrix $\mathbf{A}$ are recovered as follows

$$\mathbf{\Phi} = \mathbf{U}\mathbf{W}, \tag{16}$$

where $\mathbf{\Phi} \in \mathbb{C}^{n\times r}$. Finally, $\mathbf{b}$, is computed as

$$\mathbf{b} = \mathbf{\Phi}^\dagger \mathbf{x_1}, \tag{17}$$

where $\mathbf{b} \in \mathbb{C}^{r\times 1}$. The standard DMD procedure is summarized in Algorithm 1.

Algorithm 1 Dynamic Mode Decomposition

Input: $\mathbf{X} = [\,\mathbf{x_1}\ \mathbf{x_2}\ \mathbf{x_3} \dots\ \mathbf{x_m}] \in \mathbb{R}^{n\times m}$.
Output: $\mathbf{\Phi} \in \mathbb{C}^{n\times r}$, $\mathbf{\Lambda} \in \mathbb{C}^{r\times r}$, $\mathbf{W} \in \mathbb{C}^{r\times r}$, $\mathbf{b} \in \mathbb{C}^{r\times 1}$.
1: $\mathbf{X_1} \leftarrow [\,\mathbf{x_1}\ \mathbf{x_2}\ \mathbf{x_3} \dots\ \mathbf{x_{m-1}}]$, $\mathbf{X_1} \in \mathbb{R}^{n\times(m-1)}$,
$\mathbf{X_2} \leftarrow [\,\mathbf{x_2}\ \mathbf{x_3}\ \mathbf{x_4} \dots\ \mathbf{x_m}]$, $\mathbf{X_2} \in \mathbb{R}^{n\times(m-1)}$.
2: $[\mathbf{U}, \mathbf{\Sigma}, \mathbf{V}]$ = `svd` ($\mathbf{X_1}$) ,
$\mathbf{U} \in \mathbb{R}^{n\times r}, \mathbf{\Sigma} \in \mathbb{R}^{r\times r}, \mathbf{V} \in \mathbb{R}^{(m-1)\times r}$.
3: $\tilde{\mathbf{A}} \leftarrow \mathbf{U}^*\mathbf{X_2}\mathbf{V}\mathbf{\Sigma}^{-1}$, $\tilde{\mathbf{A}} \in \mathbb{R}^{r\times r}$
4: $[\mathbf{W}, \mathbf{\Lambda}] = \mathtt{eig}(\tilde{\mathbf{A}})$.
5: $\mathbf{\Phi} \leftarrow \mathbf{U}\mathbf{W}$.
6: $\mathbf{b} \leftarrow \mathbf{\Phi}^\dagger \mathbf{x_1}$.

A. Data Stacking

Suppose that there is one measurement channel. The data matrix $\mathbf{X}$ will be a row vector. This certainly makes estimation difficult. To construct a data matrix, stacking technique is used to obtain a data matrix $\mathbf{X}$ with a higher row dimension. Augmenting the data in shift-stacking and time-delay matrix ensures more accurate solution [16]. Moreover, data stacking increases the dimension of the measurement matrix that helps capture more information from the data. The general data multi-channel form is set as follows.

$$\begin{aligned}\mathbf{X_{aug}} &= \begin{bmatrix} \mathbf{X}_1^{m-(s-1)} \\ \mathbf{X}_2^{m-(s-2)} \\ \vdots \\ \mathbf{X}_s^m \end{bmatrix} \\ &= \begin{bmatrix} \mathbf{x}_1 & \mathbf{x}_2 & \cdots & \mathbf{x}_{m-(s-1)} \\ \mathbf{x}_2 & \mathbf{x}_3 & \cdots & \mathbf{x}_{m-(s-2)} \\ \vdots & \vdots & \ddots & \vdots \\ \mathbf{x}_s & \mathbf{x}_{s+1} & \cdots & \mathbf{x}_m \end{bmatrix}\end{aligned} \tag{18}$$

where $\mathbf{X_{aug}} \in \mathbb{R}^{s\cdot n\times(m-s+1)}$, and s is the stacking number. The DMD algorithm splits the augmented data into two overlapping sets:

$$\mathbf{X_{aug,1}} = \mathbf{X_{aug}}(:, 1 : m-s) \tag{19a}$$

$$\mathbf{X_{aug,2}} = \mathbf{X_{aug}}(:, 2 : m-s+1) \tag{19b}$$

where $\mathbf{X_{aug,1}}$, $\mathbf{X_{aug,2}} \in \mathbb{R}^{s\cdot n\times(m-s)}$. It can be seen that

$$\mathbf{X_{aug,2}} = \mathrm{diag}([\mathbf{A}, \cdots, \mathbf{A}])\mathbf{X_{aug,1}}.$$

With the two new data matrices, the same DMD procedure can be carried out for modal analysis.

III. Randomized Technique and DMD

Our research on real-world event data shows that to achieve accuracy, the number s for data stacking is selected to be 30 - 40% of the measurement snapshots number. This number may be greater than 200. This results in large data matrices. Data handling requires more computing time. For computing efficiency, in this paper, randomized DMD will be implemented. The objective is to replace the large-scale data matrix $\mathbf{X_{aug}} \in \mathbb{R}^{(s\cdot n)\times(m-s+1)}$ by a matrix with a smaller row dimension.

A. Randomization Method

The process of the presented randomization method is to build a new small data matrix that reflects the original data matrix with adequate quality. The randomization technique we employ was proposed by Halko et al. [24]. It consists of two stages: stage A and stage B. Moreover, two additional approaches (oversampling and power iteration scheme) are implemented to ensure the reduced data set has high quality.

1) Stage A: For the given data matrix, $\mathbf{X} \in \mathbb{R}^{n\times m}$, and the target rank $k \ll \min(m,n)$, we seek to find the optimal orthonormal basis $\mathbf{Q} \in \mathbb{R}^{n\times k}$ that holds:

$$\mathbf{X} \approx \mathbf{Q}\underbrace{\mathbf{Q}^*\mathbf{X}}_{\mathbf{H}}. \tag{20}$$

$\mathbf{H} \in \mathbb{R}^{k\times m}$ will be used to represent $\mathbf{X}$.

First, the column space of $\mathbf{X}$ is sampled. The sampling proceeds by projecting the original high-dimensional data onto a random matrix:

$$\mathbf{Y} = \mathbf{X}\mathbf{\Psi}, \tag{21}$$

where $\mathbf{\Psi} \in \mathbb{R}^{m\times k}$ is a normal Gaussian distribution matrix. $\mathbf{Y}$ is a set of linearly independent vectors that span in the range of $\mathbf{X}$. Consequently, the optimal basis $\mathbf{Q}$ can be efficiently achieved by means of QR-decomposition such that

$$\mathbf{Y} = \mathbf{Q}\mathbf{R}. \tag{22}$$

2) Stage B: Given the optimal basis $\mathbf{Q}$, the small data matrix $\mathbf{H} \in \mathbb{R}^{k\times m}$ is obtained by projecting the original matrix, $\mathbf{X}$, onto the computed basis $\mathbf{Q}$

$$\mathbf{H} = \mathbf{Q}^*\mathbf{X}. \tag{23}$$

It is worth mentioning that the original data matrix, $\mathbf{X}$, is preserved; it can be recovered as follows

$$\mathbf{X} \approx \mathbf{Q}\mathbf{H}. \tag{24}$$

3) Oversampling: to ensure the column space of $\mathbf{Q}$ spans in $\mathbf{X}$ with high probability, extra samples are added from the measurements via the random matrix. Therefore, we have $\mathbf{\Psi} \in \mathbb{R}^{m\times l}$, where $l = k+p$. The parameter k is the rank of $\mathbf{X}$ and p denotes the extra samples. Reference [24] suggests setting p to 5 or 10 is sufficient to achieve correct results. In our case studies, we set $p = 10$.

4) Power Iteration Scheme: in case the data matrix, $\mathbf{X}$, has a slowly decaying singular value spectrum, the quality of the basis $\mathbf{Q}$ declines. The power iteration scheme dramatically fastens the singular value spectrum decaying [23]. Power iteration scheme is implemented as follows.

$$\mathbf{Y} = \left((\mathbf{X}\mathbf{X}^*)^q\,\mathbf{X}\right)\mathbf{\Psi}, \tag{25}$$

where q is an integer number that represents the power iterations. Although the cases in this paper have high noises, setting $q = 2$ leads a sufficiently fast singular value spectrum. Higher value of q conveys a more accurate solution, but at the cost of extra computation. If $\mathbf{X}$ is factorized using SVD and $\mathbf{X} = \mathbf{U}\mathbf{\Sigma}\mathbf{V}^*$, then (25) becomes the following: $\mathbf{Y} = \left((\mathbf{X}\mathbf{X}^*)^q\,\mathbf{X}\right)\mathbf{\Psi} = \mathbf{U}\mathbf{\Sigma}^{2q+1}\mathbf{V}^*\mathbf{\Psi}$. The randomized technique is demonstrated in Algorithm 2.

Algorithm 2 Randomized technique [23]

Input: $\mathbf{X} \in \mathbb{R}^{n\times m}$, $k \ll \min(m,n)$, p, q
Output: $\mathbf{H} \in \mathbb{R}^{l\times m}$, $\mathbf{Q} \in \mathbb{R}^{n\times l}$

$l \leftarrow k + p$
$\mathbf{\Psi} \leftarrow \mathtt{rand}(m, l)$
$\mathbf{Y} \leftarrow \mathbf{X}\mathbf{\Psi}$, $\mathbf{Y} \in \mathbb{R}^{n\times l}$
for $k = 1, \ldots, q$ **do**
  $[\mathbf{Q}, \sim] = \mathtt{qr}(\mathbf{Y})$
  $[\mathbf{Z}, \sim] = \mathtt{qr}(\mathbf{X}^*\mathbf{Q})$
  $\mathbf{Y} = \mathbf{X}\mathbf{Z}$
end for
$[\mathbf{Q}, \sim] = \mathrm{qr}(\mathbf{Y})$
$\mathbf{H} \leftarrow \mathbf{Q}^*\mathbf{X}$

B. Randomized DMD

While data stacking improves DMD performance, it increases the computation cost. This section provides computation enhancement to the algorithm process. The methodology relies on including the randomization technique into the DMD steps. This method is proposed by Erichson et al. [23]. The result of the rDMD matches standard DMD. The rDMD is implemented after computing the optimal orthonormal basis $\mathbf{Q}$ from Algorithm 2. The high-dimensional measurement snapshots are projected onto $\mathbf{Q}$ as follows.

$$\mathbf{h}_1, \mathbf{h}_2, \ldots, \mathbf{h}_m := \mathbf{Q}^*\mathbf{x}_1, \mathbf{Q}^*\mathbf{x}_2, \ldots, \mathbf{Q}^*\mathbf{x}_m \in \mathbb{R}^l. \tag{26}$$

The new low-dimensional snapshots are gathered into two overlapping matrices just as in (8)

$$\mathbf{H}_1^{m-1} = \begin{bmatrix} | & | & & | \\ \mathbf{h}_1 & \mathbf{h}_2 & \cdots & \mathbf{h}_{m-1} \\ | & | & & | \end{bmatrix}, \tag{27a}$$

$$\mathbf{H}_2^{m} = \begin{bmatrix} | & | & & | \\ \mathbf{h}_2 & \mathbf{h}_3 & \cdots & \mathbf{h}_{m} \\ | & | & & | \end{bmatrix}, \tag{27b}$$

where $\mathbf{H}_1^{m-1}$, $\mathbf{H}_2^{m} \in l \times (m-1)$. Then, the dynamics matrix that maps the two low-dimensional sets is computed using least-squares estimation:

$$\begin{aligned} \mathbf{A}_\mathbf{h} &= \mathbf{H}_2^m(\mathbf{H}_1^{m-1})^\dagger \\ &= \mathbf{H}_2^m\mathbf{V}\mathbf{\Sigma}^{-1}\mathbf{U}^*, \end{aligned} \tag{28}$$

where $\mathbf{A}_\mathbf{h} \in \mathbb{R}^{l\times l}$, $\mathbf{U} \in \mathbb{R}^{l\times k}, \mathbf{\Sigma} \in \mathbb{R}^{k\times k}$, and $\mathbf{V} \in \mathbb{R}^{(m-1)\times k}$. $\mathbf{U}, \mathbf{\Sigma}$, and $\mathbf{V}$ are the truncated SVD components of $\mathbf{H_1}^{(m-1)}$. $\mathbf{A_h}$ is projected onto $\mathbf{U}$ basis to make it even smaller:

$$\tilde{\mathbf{A}}_h = \mathbf{U}^*\mathbf{A}_\mathbf{h}\mathbf{U} = \mathbf{U}^*\mathbf{H}_2^m\mathbf{V}\mathbf{\Sigma}^{-1}, \tag{29}$$

where $\tilde{\mathbf{A}}_h \in \mathbb{R}^{k\times k}$. Next, the eigendecomposition is implemented to obtain the system eigenvalues and eigenvectors:

$$\tilde{\mathbf{A}}_h\mathbf{W}_\mathbf{h} = \mathbf{W}_\mathbf{h}\mathbf{\Lambda}_\mathbf{h}, \tag{30}$$

where $\mathbf{\Lambda}_\mathbf{h} \in \mathbb{C}^{k\times k}$, and $\mathbf{W}_\mathbf{h} \in \mathbb{C}^{k\times k}$. The DMD modes are recovered as

$$\mathbf{\Phi}_\mathbf{h} = \mathbf{Q}\mathbf{U}\mathbf{W}_\mathbf{h}, \tag{31}$$

TABLE I: Real-world event descriptions.

Case #	Date	PMU	Type	Frequency (Hz)
1	June 17, 2016	ISO-NE	System-wide mode	0.27
2	Oct 3, 2017	ISO-NE	Wide-spread	0.08, 0.15 0.31
3	Jul. 20, 2017	ISO-NE	Regional	1.13

where $\mathbf{\Phi_h} \in \mathbb{C}^{n\times k}$. The vector mode amplitudes, $\mathbf{b_h}$, is evaluated as

$$\mathbf{b_h} = \mathbf{\Phi_h}^{\dagger}\mathbf{Q}\mathbf{h_1}, \tag{32}$$

where $\mathbf{b_h} \in \mathbb{C}^{k\times 1}$. The randomized dynamic mode decomposition is outlined in Algorithm 3.

Algorithm 3 Randomized Dynamic Mode Decomposition

Input: $\mathbf{H} = [\,\mathbf{h_1}\ \mathbf{h_2}\ \mathbf{h_3}\ldots\ \mathbf{h_m}] \in \mathbb{R}^{l\times m}$, $\mathbf{Q} \in \mathbb{R}^{n\times l}$

Output: $\mathbf{\Phi_h} \in \mathbb{C}^{n\times k}$, $\mathbf{\Lambda_h} \in \mathbb{C}^{k\times k}$, $\mathbf{W_h} \in \mathbb{C}^{k\times k}$, $\mathbf{b_h} \in \mathbb{C}^{k\times 1}$.

1: $\mathbf{H_1} \leftarrow [\,\mathbf{h_1}\ \mathbf{h_2}\ \mathbf{h_3}\ldots\ \mathbf{h_{m-1}}]$, $\mathbf{H_1} \in \mathbb{R}^{l\times m-1}$, $\mathbf{H_2} \leftarrow [\,\mathbf{h_2}\ \mathbf{h_3}\ \mathbf{h_4}\ldots\ \mathbf{h_h}]$, $\mathbf{H_2} \in \mathbb{R}^{l\times m-1}$.

2: $[\mathbf{U}, \mathbf{\Sigma}, \mathbf{V}]$ = svd ($\mathbf{H_1}$) , $\mathbf{U} \in \mathbb{R}^{l\times k}, \mathbf{\Sigma} \in \mathbb{R}^{k\times k}, \mathbf{V} \in \mathbb{R}^{m-1\times k}$.

3: $\tilde{\mathbf{A}}_h \leftarrow \mathbf{U}^*\mathbf{H_2}\mathbf{V}\mathbf{\Sigma}^{-1}$, $\tilde{\mathbf{A}}_h \in \mathbb{R}^{k\times k}$

4: $[\mathbf{W_h}, \mathbf{\Lambda_h}] = \mathtt{eig}(\tilde{\mathbf{A}}_h)$.

5: $\mathbf{\Phi_h} \leftarrow \mathbf{QUW_h}$.

6: $\mathbf{b_h} \leftarrow \mathbf{\Phi_h}^{\dagger}\mathbf{Q}\mathbf{h_1}$.

In the following section, DMD and rDMD will be demonstrated on real-world event data analysis. All calculations were performed in MATLAB on a laptop with an Intel Core i7 CPU and 16Gb of memory.

IV. Real-World Oscillation Event Case Studies

This section presents implementation of DMD and rDMD on three real-world oscillation events. These events occurred in ISO New England, a North-East part of the Eastern Interconnection in the U.S., shown in Fig. 1. The ISO New England has peak load of 26,000 MW. Data and brief descriptions of the three events are from Test Cases Library of Power System Sustained Oscillations [5]. The sampling period, Δt, is 0.033 second. Table I presents the three events descriptions from [5].

Fig. 2 present the voltage magnitudes during the events recorded by PMUs.

A. Oscillation Event 1

On June 17, 2016, an emergency shutdown due to control failure of a nuclear reactor occurred in the Grand Gulf Nuclear Station that is in Area 2. The cause of the failure was hydraulic control valve malfunctioning. As a result, 65 percent of the power load was dropped of the system, and a forced oscillation frequency around 0.28 Hz was imposed in the system for about 45 minutes [25]. 32 of the PMUs recorded the event, the voltage magnitude signals are shown in Fig. 2a.

Data from 40 to 60 seconds are used for analysis. Without shift-stacking, the DMD is unable to identify the system and reconstruct the signals, as shown in Fig. 3a. Shift-stacking the event data enables the DMD to accurately identify the

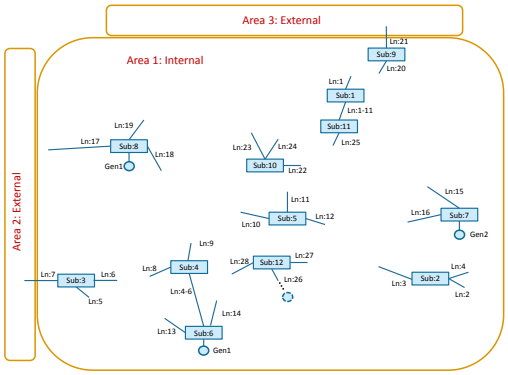

Fig. 1: The ISO New England map [5].

TABLE II: Real-World Event 1: Computation Details

Event 1: Voltage Magnitudes	**DMD**	**rDMD**
Matrix Dimension	8000×456	26×456
Computation Time (s)	0.2282	0.0079

system modes and reconstruct the signals from the DMD's components, as shown in Fig. 3b. For this case, excellent matching of reconstructed and original signals is achieved with the shift-stacking number s at 250. The data matrix's dimension changes from (32×705) to (8000×456) that is from $(n \times m)$ to $(n \cdot s \times m - s + 1)$. The proposed rDMD reduces the size to (26×456), which is $(k + p \times m - s + 1)$, while analysis accuracy is preserved.

The randomized decomposition computation time is 0.0165 s. The DMD and rDMD computation details are shown in Table II.

Since the measurement data are expected to be corrupted by noises, we examine the singular value energies before we truncate the model through the SVD elements. Fig. 4 shows the Event 1 singular value energies and cumulative energies. Setting the DMD rank to 16 holds 99.95% of the data information. Consequently, both the DMD and rDMD identify 16 eigenvalues that are shown Fig. 5.

The DMD spectrum determines the dominant modes in the analyzed system; for this case, the DMD spectrum is shown in Fig. 6. The dominant oscillation mode is at 0.28 Hz, which matches NERC report [25].

B. Oscillation Event 2

On October 3, 2017 inter-area oscillations of 0.08 Hz, 0.15 Hz, and 0.31 Hz initiated and dispersed in the New England power system. The oscillations source was at an external area (Area 3), where an issue had occurred on a large generator governor. The oscillations lasted in the network for about 5 minutes. For this case, 23 of the PMUs captured the event, the voltage magnitude measurements are shown in Fig. 2b. Both DMD and rDMD are implemented on a time window from 250s to 280s for all the given PMU voltage magnitude signals.

The DMD without shift-stacking the data is incapable to identify the event and reconstruct the signals, as appeared in Fig. 7a. On the other hand, the DMD with shift-stacking the

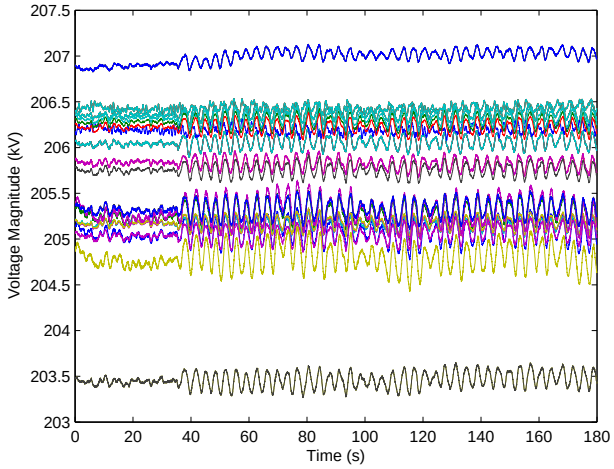

(a) Event 1.

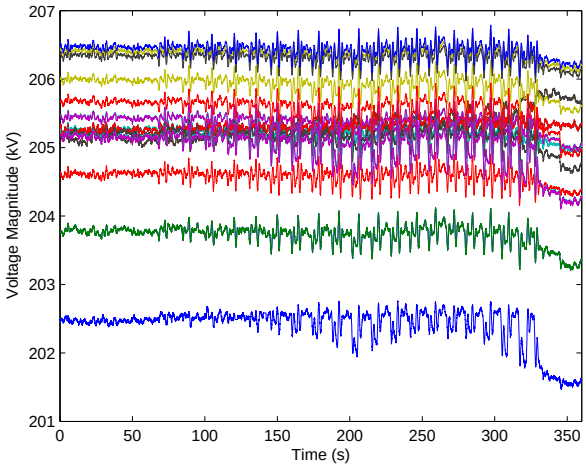

(b) Event 2.

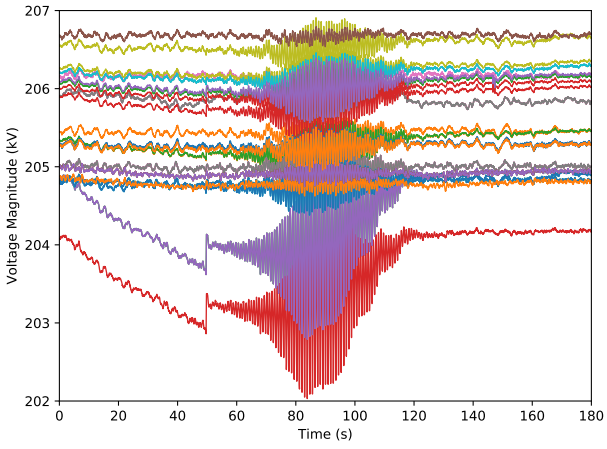

(c) Event 3.

Fig. 2: Phase-to-ground voltage magnitudes during the oscillatory events.

data has the ability to identify and reconstruct the signals, as shown in Fig. 7b. The analyzed data size is (22×910). The DMD reconstructed signals match the original signals with a stack number $s = 350$. The randomized decomposition computation time is 0.0358 s. The DMD and rDMD computation details are shown in Table III.

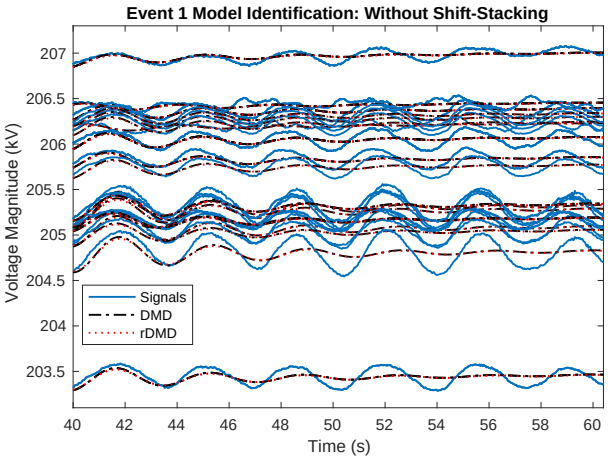

(a)

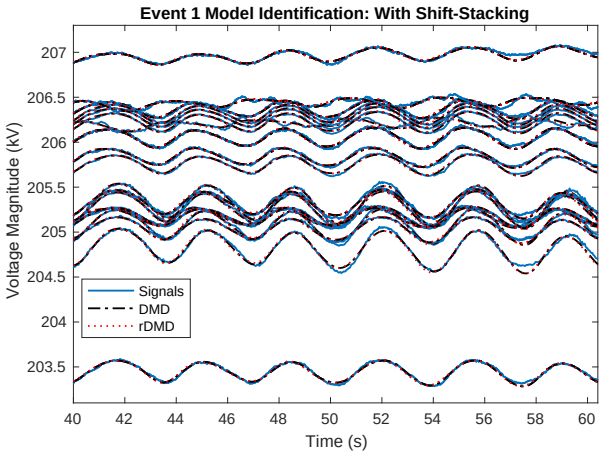

(b)

Fig. 3: Comparison of data stacking for Event 1.

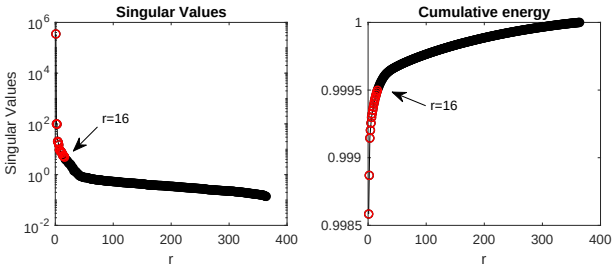

Fig. 4: Event 1: Singular value energies and cumulative energy.

TABLE III: Real-World Event 2: Computation Details

Event 2: Voltage Magnitudes	**DMD**	**rDMD**
Matrix Dimension	7700×561	40×561
Computation Time (s)	0.3008	0.0107

For this case, the cumulative energy of the first 30 of the singular values is 99.94%. By comparison with Event 1 case in which the first 16 of the singular values have a cumulative energy of 99.95%, one can conclude that Event 2 includes more dynamics and noises than Event 1. According to the singular values, the DMD rank is set to 30. Therefore, the DMD and rDMD identify 30 eigenvalues that are shown in

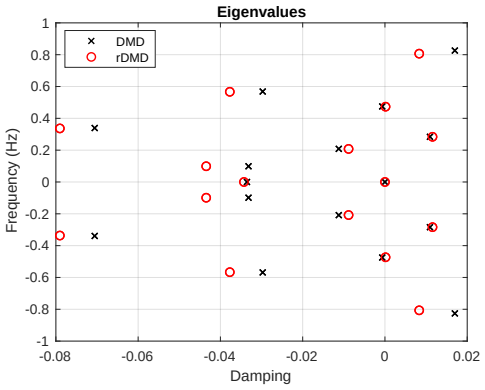

Fig. 5: Event 1: Eigenvalues identified by DMD and rDMD.

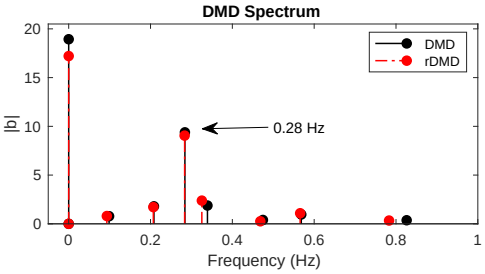

Fig. 6: DMD Spectrum of Event 1.

TABLE IV: Real-World Event 3: Algorithm Computation Time

Algorithm	rDMD	DMD	MP	Prony	ERA
Time (s)	0.0769	0.1467	0.7310	1.8357	2.3675

Fig. 8. They show a close match.

The Event 2 DMD spectrum, shown in Fig. 9, indicates that the event dominant modes are 0.0833 Hz, 0.1489 Hz, and 0.3056 Hz. The identified modes have frequencies agreeing with the info in Table I.

C. Oscillation Event 3: Comparison with classical methods

On July 20, 2017, a disturbance in a large generator initiated growing regional oscillations in Area 1. The number of the PMUs that recorded the event is 35, the voltage magnitude measurements are shown in Fig. 2c. In this case study, we show a comparison between the DMD/rDMD and the classical identification methods that are Prony, Matrix Pencil (MP), and ERA. The analyzed ringdown response is the voltage magnitude from 51 to 65 second. The signal reconstruction of the tested methods are compared with PMU voltage in Fig. 10. The data matrix has 20 effective singular values and correspondingly the rank of all the tested methods is 20. The mismatching error of all of the algorithms are shown in Fig. 11, and their computation times are in Table IV. It can be seen that the mismatching errors of DMD and rDMD are the lowest, which indicates DMD and rDMD lead to most accurate reconstructed signals.

D. Mode shape analysis for the dominant mode of Event 1 and Event 3

Mode shape analysis based on frequency measurements has been used in the industry to distinct oscillation type,

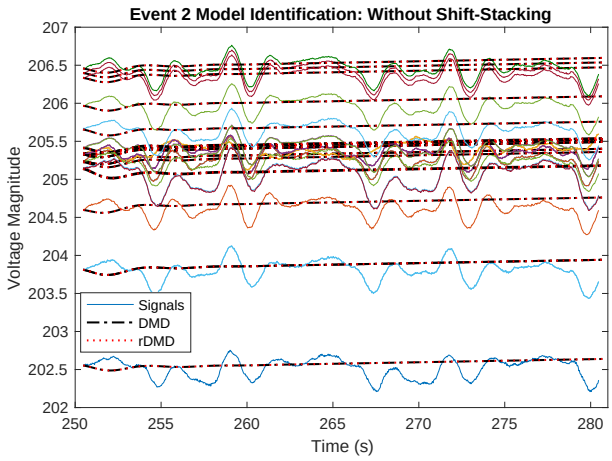

(a)

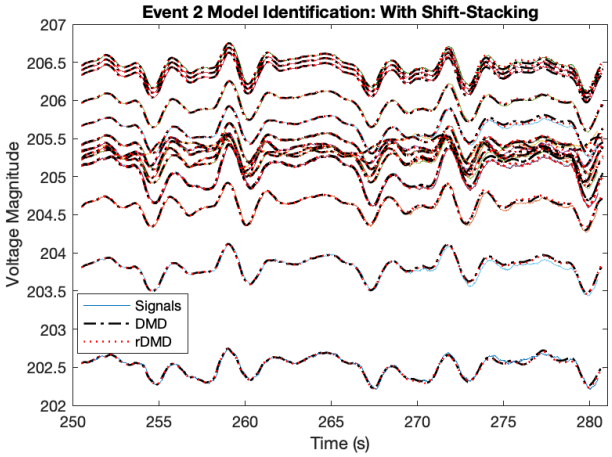

(b)

Fig. 7: Comparison of data stacking for Event 2 signal reconstruction. (a) Without stacking. (b) With data stacking.

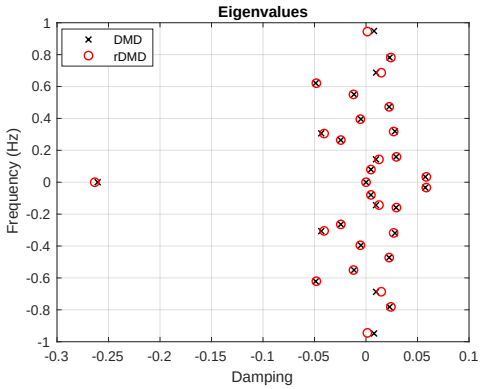

Fig. 8: Event 2: Eigenvalues identified by DMD and rDMD.

e.g., [25]. In this subsection, frequency measurements will be used for DMD analysis and further mode shape (ϕ_i of the ith mode) of the dominant modes will be plotted for oscillation type analysis. Fig. 12a and Fig. 12b present the frequency measurements of the two events used for DMD analysis. For Event 1, 20 seconds data are used while for Event 3, 40 seconds data are used. Randomized DMD successfully identifies eigenvalues and the reconstructed signals are also shown in Fig. 12a and Fig. 12b.

The dominant mode of Event 1 is the 0.28 Hz mode which

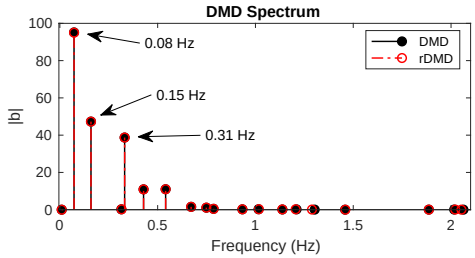

Fig. 9: DMD Spectrum of Event 2.

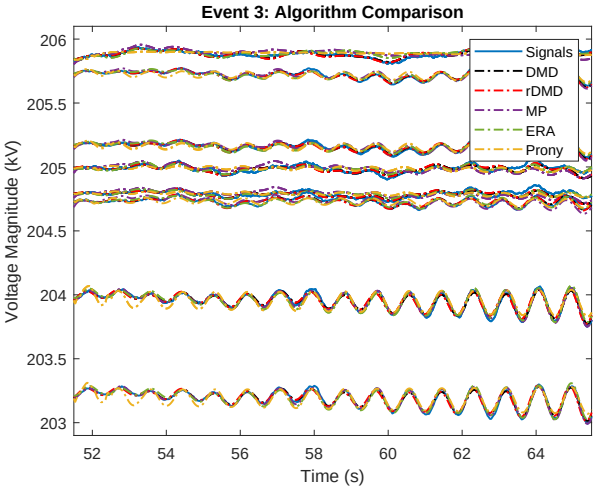

Fig. 10: Event 3: Algorithm comparison.

has been also identified using the voltage magnitude data while the dominant mode of Event 3 is a 1.14 Hz mode. A complete s-domain eigenvalue location plot based on Event 3 data is shown in Fig. 13. The dominant mode is the 1.14 Hz mode.

Mode shapes corresponding to the dominant mode for each event are plotted in Fig. 14. It can be seen that for Event 1 for the 0.28 Hz mode, mode shapes corresponding to the substations at New England have almost the same angles. That is, for this mode, the entire New England can be treated as a single generator. This mode is indeed an inter-area oscillation

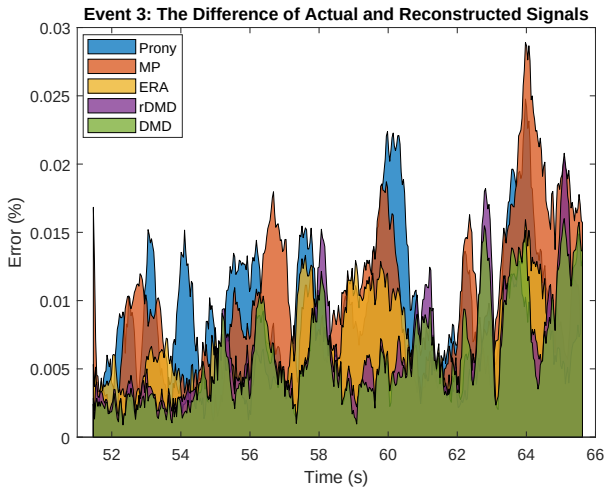

Fig. 11: Event 3: Algorithm reconstruction signal error.

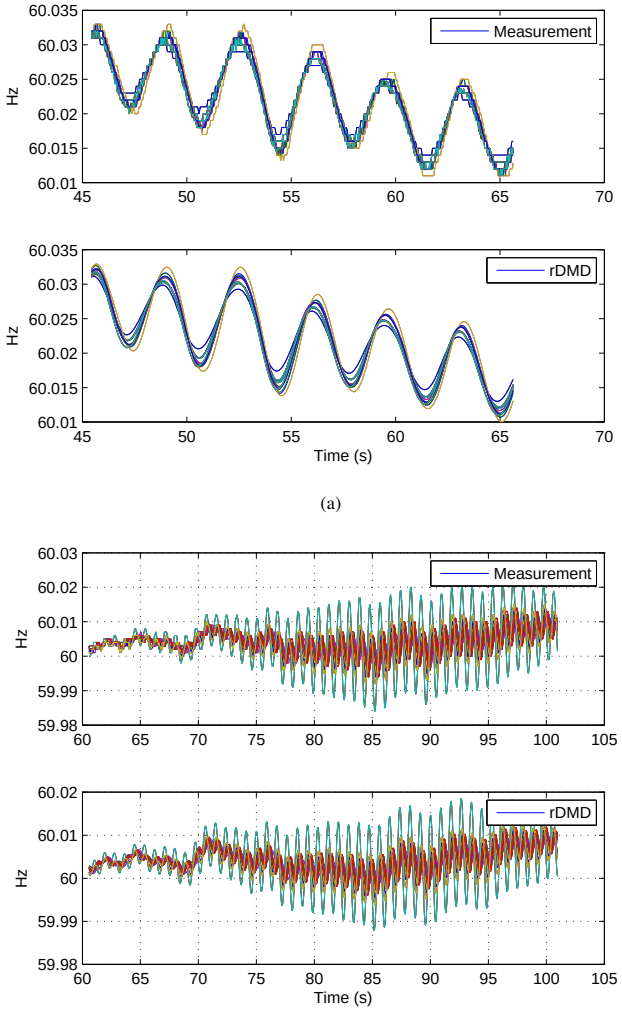

Fig. 12: (12a) Event 1 frequency measurement and reconstructed signals. Rank is assumed as 16. Data stacking number is 350. (12b Event 3 frequency measurement and reconstructed signals. Rank is assumed as 20 and data stacking number is 550.

mode. On the other hand, mode shape plot of the 1.14 Hz mode of Event 3 indicates that the mode shape vectors of New England substations are not contained in a cone with a small angle. Rather, the angles are quite different. [5] identified the dominant mode of Event 3 as a regional mode. This feature is also confirmed by Fig. 14b.

V. Conclusion

In this paper, DMD is implemented in real-world inter-area oscillation event analysis to identify the oscillation modes and distinct their nature. This paper improves DMD for modal analysis of power grids in two aspects: enhanced accuracy and reduced computing cost. Enhanced accuracy is achieved by the use of data shift-stacking technique, which results in a data matrix with a much larger size. To reduce computing cost, randomized linear algebra technique creates a new data matrix with much less row dimension while having data information preserved. The resulting randomized DMD is implemented in this paper for oscillation analysis. Three real-world oscillation

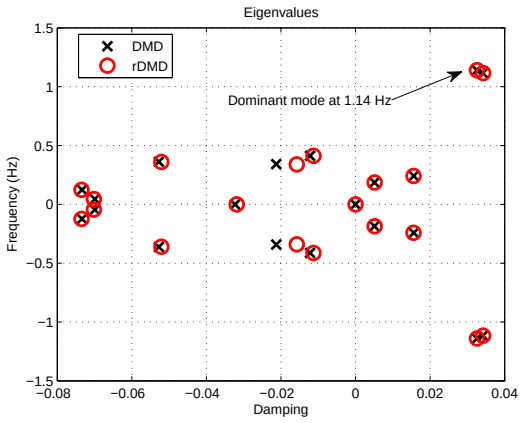

Fig. 13: Identified eigenvalues based on Event 3 data.

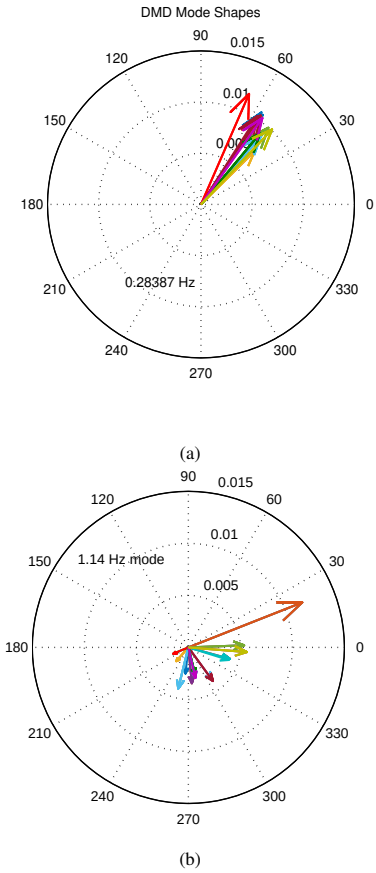

(a)

(b)

Fig. 14: (a) Event 1 0.28 Hz mode's mode shape. (b) Event 3 1.14 Hz mode's mode shape.

event data have been used for case studies to demonstrate the excellent modal identification capability of rDMD.

REFERENCES

[1] D. N. Kosterev, C. W. Taylor, and W. A. Mittelstadt, "Model validation for the august 10, 1996 wscc system outage," *IEEE transactions on power systems*, vol. 14, no. 3, pp. 967–979, 1999.

[2] Q. F. Zhang, X. Luo, E. Litvinov, N. Dahal, M. Parashar, K. Hay, and D. Wilson, "Advanced grid event analysis at iso new england using phasorpoint," in *2014 IEEE PES General Meeting— Conference & Exposition*. IEEE, 2014, pp. 1–5.

[3] M. Shahraeini, M. H. Javidi, and M. S. Ghazizadeh, "Comparison between communication infrastructures of centralized and decentralized wide area measurement systems," *IEEE Transactions on Smart Grid*, vol. 2, no. 1, pp. 206–211, 2010.

[4] S. Maslennikov, B. Wang, Q. Zhang, E. Litvinov *et al.*, "A test cases library for methods locating the sources of sustained oscillations," in *2016 IEEE Power and Energy Society General Meeting (PESGM)*. IEEE, 2016, pp. 1–5.

[5] Test cases library of power system sustained oscillations. http://web.eecs.utk.edu/~kaisun/Oscillation/actualcases.html, July 2019.

[6] J. F. Hauer, C. Demeure, and L. Scharf, "Initial results in prony analysis of power system response signals," *IEEE Transactions on power systems*, vol. 5, no. 1, pp. 80–89, 1990.

[7] L. L. Grant and M. L. Crow, "Comparison of matrix pencil and prony methods for power system modal analysis of noisy signals," in *2011 North American Power Symposium*. IEEE, 2011, pp. 1–7.

[8] L. Fan, "Data fusion-based distributed prony analysis," *Electric Power Systems Research*, vol. 143, pp. 634–642, 2017.

[9] Y. Hua and T. K. Sarkar, "Matrix pencil method for estimating parameters of exponentially damped/undamped sinusoids in noise," *IEEE Transactions on Acoustics, Speech, and Signal Processing*, vol. 38, no. 5, pp. 814–824, 1990.

[10] J. Sanchez-Gasca, "Computation of turbine-generator subsynchronous torsional modes from measured data using the eigensystem realization algorithm," in *2001 IEEE Power Engineering Society Winter Meeting. Conference Proceedings (Cat. No. 01CH37194)*, vol. 3. IEEE, 2001, pp. 1272–1276.

[11] Y. Susuki and I. Mezić, "Nonlinear koopman modes and power system stability assessment without models," *IEEE Transactions on Power Systems*, vol. 29, no. 2, pp. 899–907, 2013.

[12] A. R. Borden and B. C. Lesieutre, "Variable projection method for power system modal identification," *IEEE Transactions on Power Systems*, vol. 29, no. 6, pp. 2613–2620, 2014.

[13] M. Crow, M. Gibbard, A. Messina, J. Pierre, J. Sanchez-Gasca, D. Trudnowski, and D. Vowles, "Identification of electromechanical modes in power systems," *IEEE Task Force Report, Special Publication TP462*, 2012.

[14] A. Almunif, L. Fan, and Z. Miao, "A tutorial on data-driven eigenvalue identification: Prony analysis, matrix pencil, and eigensystem realization algorithm," *International Transactions on Electrical Energy Systems*, vol. 30, no. 4, p. e12283, 2020.

[15] P. J. Schmid, "Dynamic mode decomposition of numerical and experimental data," *Journal of fluid mechanics*, vol. 656, pp. 5–28, 2010.

[16] J. N. Kutz, S. L. Brunton, B. W. Brunton, and J. L. Proctor, *Dynamic mode decomposition: data-driven modeling of complex systems*. SIAM, 2016.

[17] E. Barocio, B. C. Pal, N. F. Thornhill, and A. R. Messina, "A dynamic mode decomposition framework for global power system oscillation analysis," *IEEE Transactions on Power Systems*, vol. 30, no. 6, pp. 2902–2912, 2015.

[18] S. Mohapatra and T. J. Overbye, "Fast modal identification, monitoring, and visualization for large-scale power systems using dynamic mode decomposition," in *2016 Power Systems Computation Conference (PSCC)*. IEEE, 2016, pp. 1–7.

[19] J. J. Ramos and J. N. Kutz, "Dynamic mode decomposition and sparse measurements for characterization and monitoring of power system disturbances," *arXiv preprint arXiv:1906.03544*, 2019.

[20] A. Alassaf and L. Fan, "Dynamic mode decomposition in various power system applications," in *2019 North American Power Symposium (NAPS)*, 2019, pp. 1–6.

[21] A. Saldaña, E. Barocio, A. Messina, J. Ramos, R. J. Segundo, and G. Tinajero, "Monitoring harmonic distortion in microgrids using dynamic mode decomposition," in *2017 IEEE Power & Energy Society General Meeting*. IEEE, 2017, pp. 1–5.

[22] P. Sharma, B. Huang, V. Ajjarapu, and U. Vaidya, "Data-driven identification and prediction of power system dynamics using linear operators," in *2019 IEEE Power & Energy Society General Meeting (PESGM)*. IEEE, 2019, pp. 1–5.

[23] N. B. Erichson, L. Mathelin, J. N. Kutz, and S. L. Brunton, "Randomized dynamic mode decomposition," *SIAM Journal on Applied Dynamical Systems*, vol. 18, no. 4, pp. 1867–1891, 2019.

[24] N. Halko, P.-G. Martinsson, and J. A. Tropp, "Finding structure with randomness: Probabilistic algorithms for constructing approximate matrix decompositions," *SIAM review*, vol. 53, no. 2, pp. 217–288, 2011.

[25] NERC. Interconnection oscillation analysis reliability assessment , july 2019. https://www.nerc.com/comm/PC/SMSResourcesDocuments/\Interconnection_Oscillation_Analysis.pdf,

Abdullah Alassaf (S'15) received the B.S. degree in electrical engineering from the University of Hail, Hail, Saudi Arabia, in 2013, and the M.S. degree in electrical engineering from the University of South Florida, Tampa, FL in 2017, where he is currently working toward the Ph.D. degree. He is with the Department of Electrical Engineering, University of Hail, Saudi Arabia,. His current research interests include power system dynamics and control.

Lingling Fan (SM'08) received the B.S. and M.S. degrees in electrical engineering from Southeast University, Nanjing, China, in 1994 and 1997, respectively, and the Ph.D. degree in electrical engineering from West Virginia University, Morgantown, in 2001.

Currently, she is an Associate Professor with the University of South Florida, Tampa, where she has been since 2009. She was a Senior Engineer in the Transmission Asset Management Department, Midwest ISO, St. Paul, MN, form 2001 to 2007, and an Assistant Professor with North Dakota State University, Fargo, from 2007 to 2009. Her research interests include power systems and power electronics. Dr. Fan serves as the editor-in-chief for IEEE Electrification Magazine and an editor for IEEE transactions on Energy Conversion.